Influence of the Size of Supertyphoon Megi (2010) on SST Cooling

IAM-FEI PUN

Graduate Institute of Hydrological and Oceanic Sciences, National Central University, Taoyuan, Taiwan

I.-I. LIN, CHUN-CHI LIEN, AND CHUN-CHIEH WU

Department of Atmospheric Sciences, National Taiwan University, Taipei, Taiwan

(Manuscript received 28 February 2017, in final form 13 December 2017)

ABSTRACT

Supertyphoon Megi (2010) left behind two very contrasting SST cold-wake cooling patterns between the Philippine Sea (1.5°C) and the South China Sea (7°C). Based on various radii of radial winds, the authors found that the size of Megi doubles over the South China Sea when it curves northward. On average, the radius of maximum wind (RMW) increased from 18.8 km over the Philippine Sea to 43.1 km over the South China Sea; the radius of 64-kt (33 m s^{-1}) typhoon-force wind (R64) increased from 52.6 to 119.7 km; the radius of 50-kt (25.7 m s^{-1}) damaging-force wind (R50) increased from 91.8 to 210 km; and the radius of 34-kt (17.5 m s^{-1}) gale-force wind (R34) increased from 162.3 to 358.5 km. To investigate the typhoon size effect, the authors conduct a series of numerical experiments on Megi-induced SST cooling by keeping other factors unchanged, that is, typhoon translation speed and ocean subsurface thermal structure. The results show that if it were not for Megi's size increase over the South China Sea, the during-Megi SST cooling magnitude would have been 52% less (reduced from 4° to 1.9°C), the right bias in cooling would have been 60% (or 30 km) less, and the width of the cooling would have been 61% (or 52 km) less, suggesting that typhoon size is as important as other well-known factors on SST cooling. Aside from the size effect, the authors also conduct a straight-track experiment and find that the curvature of Megi contributes up to 30% (or 1.2°C) of cooling over the South China Sea.

1. Introduction

The sea surface temperature (SST) cooling is one highly noticeable ocean response to a moving typhoon (Price 1981; Sanford et al. 1987; Cione and Uhlhorn 2003; Lin et al. 2003; Walker et al. 2005; D'Asaro et al. 2007, 2014). Such typhoon-induced cooling has long been an important topic for both oceanographers and meteorologists because of its significant impact on the ocean dynamics and atmosphere. Over the last three decades, observational studies (e.g., Leipper 1967; Sanford et al. 1987, 2007, 2011; Shay et al. 1992, 2000; D'Asaro 2003; Lin et al. 2003; D'Asaro et al. 2007; Wu et al. 2007; Jaimes and Shay 2009; Pun et al. 2007, 2011; Uhlhorn and Shay 2012; Mrvaljevic et al. 2013; Guan et al. 2014; Hsu et al. 2017), numerical experiments (e.g., Price 1981; Price et al. 1994, 2008; Jacob et al. 2000; Wada 2005; Chen et al. 2007; Jaimes et al. 2011; Vincent et al. 2012; Yablonsky and Ginis 2013; Ko et al. 2014; Jaimes and Shay 2015; Wu et al. 2016), and multinational field campaigns (e.g., Black et al. 2007; D'Asaro et al. 2014) have been carried out to understand the characteristics and formation mechanism of the SST cooling. It is well known that SST cooling during a typhoon's intensification stage can feed back to the typhoon itself through both modulating air–sea energy fluxes and stabilizing an atmospheric boundary layer (Chang and Anthes 1979; Bender et al. 1993; Emanuel 1999; Cione et al. 2000; Shay et al. 2000; Chen et al. 2007; Lin et al. 2008, 2009; Jaimes et al. 2015; Lee and Chen 2014; Huang et al. 2015; Zheng et al. 2015; Wu et al. 2016; Huang et al. 2017). As a result, to improve the typhoon intensity prediction, the SST cooling within a typhoon core needs to be captured (Wang and Wu 2004; Lin et al. 2013; Balaguru et al. 2015; Wu et al. 2016).

Price (1981) clearly demonstrated that the cooling amplitude and spatial extent of SST cooling are mainly controlled by typhoon characteristics and oceanic factors. The former includes the typhoon's maximum surface wind, translation speed, and size; the latter is the

Corresponding author: Iam-Fei Pun, ipun@ncu.edu.tw

DOI: 10.1175/MWR-D-17-0044.1

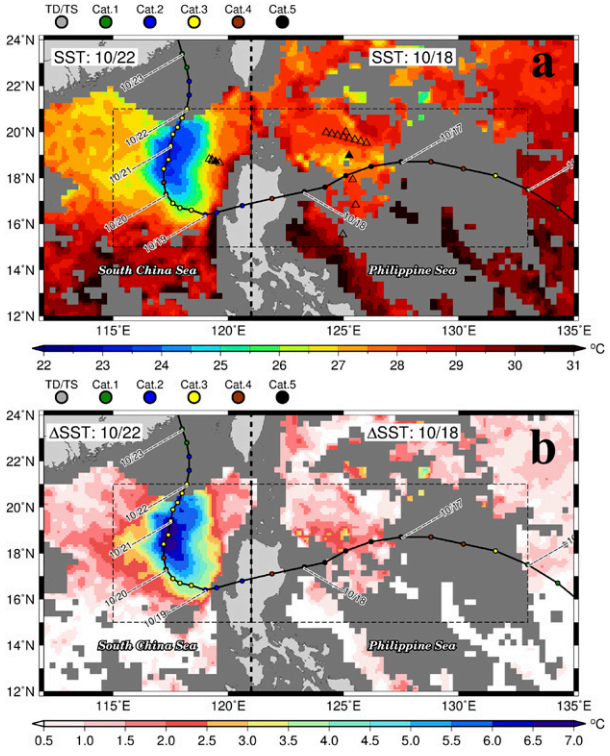

FIG. 1. (a) Daily composites of satellite microwave SST after Megi's passage on 18 Oct and 22 Oct 2010. The vertical dashed line separates the two composites, which are made from the observations from the Tropical Rainfall Measuring Mission (TRMM) Microwave Imager (TMI) and the Advanced Microwave Scanning Radiometer for Earth Observing System (AMSR-E) provided by Remote Sensing Systems (RSS). Note that there are a number of missing data (in gray) due to heavy rains of Megi. Megi's best track from IBTrACS is superimposed, color coded by the Saffir–Simpson hurricane wind scale. Triangles depict the ocean temperature profiles retrieved from the GTSPP database, while the solid triangles depict the selected profiles used for the simulations. The geographic locations and simulation domains (dashed boxes) for the Philippine Sea and the South China Sea are also shown. (b) The corresponding SST decrease map with respect to pre-Megi condition on 15 Oct 2010.

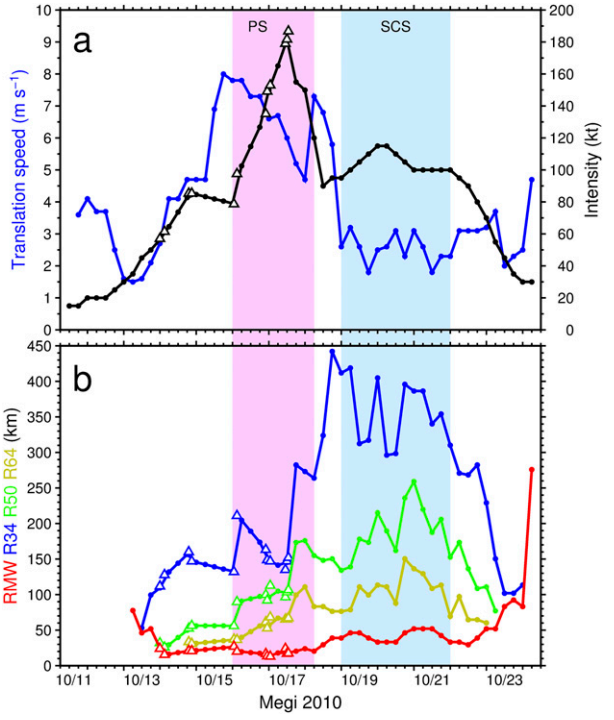

FIG. 2. (a) Intensity and translation speed and (b) radii of maximum, 64-, 50-, and 34-kt winds (i.e., RMW, R64, R50, and R34) of Megi based on multiple datasets, including airborne SFMR surface wind observations (triangles), IBTrACS best track data, and CIRA wind radii reanalysis. The pink (blue) shading indicates the simulation period for the Philippine Sea (South China Sea) experiments.

ocean's vertical thermal structure, which is often characterized by the mixed layer depth and the temperature gradient of the thermocline. From both observational and numerical studies, it is evident that upper-ocean thermal structure is a key player in modulating the SST cooling, especially when associated with ocean eddies (Shay et al. 1992, 2000; Schade and Emanuel 1999; Walker et al. 2005; Lin et al. 2005, 2008, 2014; Pun et al. 2007; Wu et al. 2007; Jaimes and Shay 2010, 2015; Jaimes et al. 2011; Vincent et al. 2012; Huang et al. 2015; Zheng et al. 2015; Huang et al. 2017).

Typically, the stronger the typhoon wind, the more the turbulent energy is transferred downward for upper-ocean mixing, and, thus, more intense SST cooling is generated (Elsberry et al. 1976; Price 1981; Lin et al. 2008; D'Asaro et al. 2014). However, the duration of the typhoon wind forcing (or residence time) is determined by the typhoon translation speed and size. Lin et al. (2009) and Mei et al. (2012) investigated the effect of translation speed on SST cooling in the western North Pacific. They found that translation speed dominates, especially in the region where the mixed layer is shallow. However, the impact of typhoon size on typhoon–ocean interactions has received less attention (Chan and Chan 2013, 2014).

Occurring late in the season, Supertyphoon Megi (2010) was one of the most intense typhoons on record (Lin et al. 2013; D'Asaro et al. 2014). Surface wind speeds of up to 186 kt (1 kt = 0.5144 m s^{-1}) were observed by the Stepped Frequency Microwave Radiometer (SFMR) on board the WC-130J aircraft from the Impact of Typhoons on the Ocean in the Pacific (ITOP) multinational field campaign (D'Asaro et al. 2011, 2014; Pun et al. 2011; Lin et al. 2013; Wu et al. 2016; Hsu et al. 2017). In addition to its extraordinary intensity, Megi contained many contrasting features in its life cycle when it traveled over the Philippine Sea and the South

TABLE 1. (top) Intensity (kt), wind radii (km), and translation speed ($m\,s^{-1}$) of Megi over the Philippine Sea from 0000 UTC 16 Oct to 1200 UTC 17 Oct based on SFMR observations. (middle) As in (top), but over the South China Sea from 0000 UTC 20 Oct to 1200 UTC 21 Oct based on IBTrACS and CIRA data. The original units for wind radii are in nautical miles (n mi; 1 n mi = 1.852 km) with a precision of 5 n mi. (bottom) The ratios of the time-averaged values between the two regimes.

Time	Intensity	RMW	R64	R50	R34	Translation speed
Philippine Sea						
0000 UTC 16 Oct	79	26.6	36.6	56.1	132.9	7.8
0600 UTC 16 Oct	103	19.7	39.9	91.1	204.7	7.8
1200 UTC 16 Oct	115	18.5	48	94.3	189.2	7.3
1800 UTC 16 Oct	127	17.4	56	97.5	173.8	7.3
0000 UTC 17 Oct	150	13.3	55.9	96.2	148.5	6.6
0600 UTC 17 Oct	165	18	66.9	105.1	141.4	6.7
1200 UTC 17 Oct	181	17.9	65.2	102.5	145.5	6
Avg	131.4	18.8	52.6	91.8	162.3	7.1
South China Sea						
0000 UTC 20 Oct	115	33.3	113.4	215.3	405.1	2.5
0600 UTC 20 Oct	115	33.3	111.1	189.8	296.3	2.6
1200 UTC 20 Oct	110	33.3	88	162	298.6	3.1
1800 UTC 20 Oct	105	46.3	150.5	236.1	395.9	2.3
0000 UTC 21 Oct	100	51.9	136.6	259.3	386.6	3.1
0600 UTC 21 Oct	100	51.9	129.6	219.9	386.6	2.6
1200 UTC 21 Oct	100	51.9	108.8	187.5	340.3	1.8
Avg	106.4	43.1	119.7	210.0	358.5	2.6
Ratio						
Philippine Sea/South China Sea	1.23	0.44	0.44	0.44	0.45	2.75
South China Sea/Philippine Sea	0.81	2.30	2.27	2.29	2.21	0.36

China Sea. The first contrasting feature is the magnitude of the SST cold wake induced by Megi (Fig. 1). Over the Philippine Sea, the SST decrease was merely about 1.5°C, even though Megi was at peak intensity with a very small eye—less than 15 km in diameter—based on WC-130J airborne radar and COSMO-SkyMed Synthetic Aperture Radar imagery composites, and surface maximum wind radius of less than 6 km, based on WC-130J SFMR measurements (D'Asaro et al. 2014). In contrast, the SST decrease exceeded 7°C over the South China Sea; the difference was nearly a factor of 5 (Fig. 1) (D'Asaro et al. 2014; Ko et al. 2014; Wu et al. 2016). The second contrast is the translation speed. Megi moved rapidly over the Philippine Sea at about $7.1\,m\,s^{-1}$ but dramatically slowed down to about $2.6\,m\,s^{-1}$ over the South China Sea (Fig. 2a). The third contrast is the typhoon size. Based on SFMR observations and satellite-based wind radii reanalysis discussed in next section, the mean wind radius of 34 kt of 162 km when Megi was over the Philippine Sea doubled to 359 km over the South China Sea (Table 1 and Fig. 2b). Note that the mean radius is defined as the azimuthal average of wind radii in the four typhoon quadrants relative to true north.

The contrast between the SST cooling induced by Megi over the Philippine Sea and the South China Sea has been attributed to the differences in upper-ocean thermal structure and Megi's translation speed (D'Asaro et al. 2014; Ko et al. 2014; Wu et al. 2016). However, it is of great interest to ask whether Megi's size, characterized by wind radii variation, also contributed to the change in the SST cooling characteristics, especially under the typhoon. To answer this question, this work aims to quantitatively assess the influence of the typhoon size on Megi-induced SST cooling over the Philippine Sea and the South China Sea through numerical simulations.

Data used in this study are described in section 2. Model and numerical experiments are introduced in section 3. Simulation results are presented in section 4. Discussions are provided in section 5. Finally, conclusions are given in section 6.

2. Data

a. Megi's radial wind structure

The time-dependent radial wind profile of Megi is necessary information in order to conduct numerical experiments. However, obtaining a continuous wind profile with typhoonwide coverage and suitable temporal resolution has been difficult. To date, the most accurate surface wind observations may be measured by typhoon-penetrating flights equipped with SFMR (Uhlhorn and Black 2003; Uhlhorn et al. 2007), but this only provides a snapshot at certain stages in the typhoon's life cycle and is not usually available for every typhoon (Black et al. 2007; D'Asaro et al. 2014).

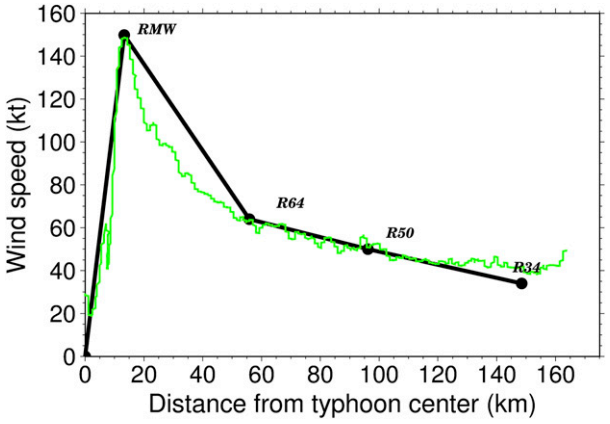

FIG. 3. Synthetic radial wind profile (black) for Megi at 0000 UTC 17 Oct 2010 that comprises four wind radii (i.e., RMW, R64, R50, and R34) based on SFMR observations (green).

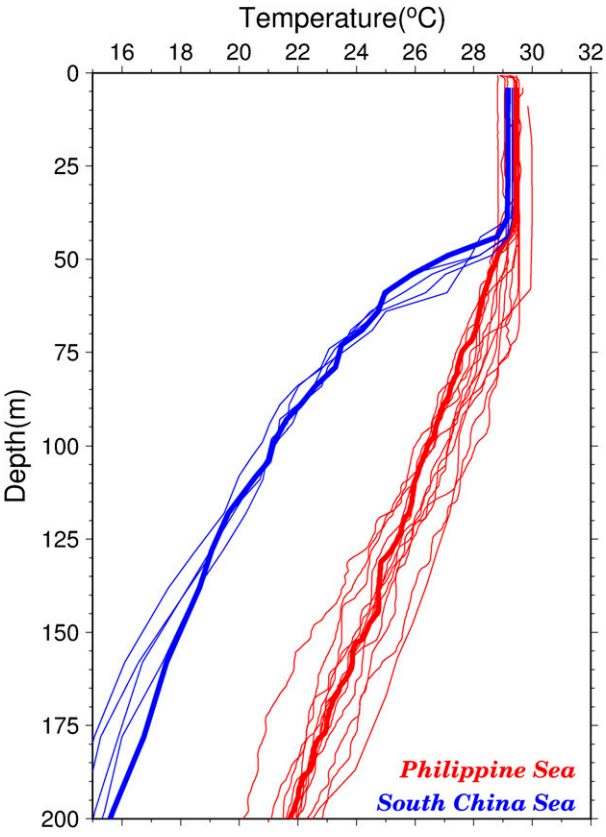

FIG. 4. In situ ocean temperature profiles in the Philippine Sea (red) and the South China Sea (blue) before the passage of Megi. It is evident that ocean subsurface thermal structure has huge differences between these two basins. The thick profiles are selected for the 3DPWP numerical experiments. The locations of the profiles are shown in Fig. 1a.

Satellite techniques provide higher spatial/temporal coverage, but it may suffer significant underestimation and uncertainty, especially the surface wind vectors under high wind conditions (Liu and Tang 1996; Chou et al. 2010). Alternatively, a better wind field for a typhoon may be generated by model assimilation with available in situ observations (Ko et al. 2014; Wu et al. 2016).

Fortunately, frequent airborne SFMR observations are available for Megi over the Philippine Sea as part of the ITOP field experiment (D'Asaro et al. 2014). In this study, we will combine multiple datasets to obtain Megi's radial wind profiles for later numerical simulations. First, Megi's 6-hourly locations are obtained from the International Best Track Archive for Climate Stewardship (IBTrACS; Knapp et al. 2010). This best track position is based on four meteorological agencies: Joint Typhoon Warning Center (JTWC), Japan Meteorological Agency (JMA), China Meteorological Administration (CMA), and Hong Kong Observatory (HKO). Second, SFMR surface wind structures from five of ITOP's WC-130J flights during 13–17 October 2010 are extracted and interpolated into regular 6-hourly intervals (Fig. 2). This SFMR dataset has been corrected for rain contamination (Klotz and Uhlhorn 2014) and archived at the Hurricane Research Division (HRD) of the U.S. National Oceanic and Atmospheric Administration (NOAA). The maximum surface wind speed of Megi is up to 186 kt, recorded by SFMR around 1300 UTC 17 October 2010 (Fig. 2a). Because of the limited observations, SFMR-derived intensity and wind radii are only available for the period between 0000 UTC 14 October and 1200 UTC 17 October, when Megi was over the Philippine Sea. For the rest of Megi's track points, JTWC best track intensity, which is also archived in IBTrACS, is applied. Finally, the remaining wind radius information is obtained from satellite-based typhoon wind radii reanalysis from the Cooperative Institute for Research in the Atmosphere (CIRA; Mueller et al. 2006). Note that the radii used here are azimuthal means.

Based on this observation-based dataset, Megi's intensity and radii for maximum winds (RMW) at 64 (R64), 50 (R50), and 34 kt (R34) are already available for every 6 h (Fig. 2). At each 6-hourly track point, these radii, together with intensity, are used to form the 6-hourly radial wind profile, which, namely, consists of the typhoon center (wind speed = 0), RMW, R64, R50, and R34. Figure 3 illustrates an exemplary profile at 0000 UTC 17 October 2010, along with SFMR observation. The translation speed is computed by a backward calculation between two 6-hourly positions.

From Fig. 2b, it is found that the size of Megi increased steadily during the rapid intensification stage over the Philippine Sea; the mean RMW, R64, R50, and

TABLE 2. Changes in variables associated with each experiment. No change in the control experiments, in which all variables are based on the observed values.

Expt	Basin	RMW	R64	R50	R34	Translation speed	Ocean subsurface condition
PS_control	Philippine Sea						
PS_size		×2.30	×2.27	×2.29	×2.21		
PS_Uh						2.6 m s^{-1}	
PS_ocean							Cold
SCS_control	South China Sea						
SCS_size		×0.44	×0.44	×0.44	×0.45		
SCS_Uh						7.1 m s^{-1}	
SCS_ocean							Warm

R34 are around 19, 53, 92, and 162 km, respectively. However, these radii sharply increase to 43, 120, 210, and 359 km, respectively, indicating the increase in Megi's size after entering the South China Sea (Table 1). The change in Megi's size appears to coincide with the change in the posttyphoon SST cooling patterns between the Philippine Sea and the South China Sea (Fig. 1). Wu et al. (2003) reported that such an increase in size was not unusual after typhoons passed through the Philippine Islands.

b. *Ocean temperature profiles*

In situ ocean temperature profiles before Megi's passage over the Philippine Sea and the South China Sea are obtained from the Global Temperature and Salinity Profile Program (GTSPP; https://www.nodc.noaa.gov/GTSPP/) (Sun et al. 2010). GTSPP seeks to collect all available ocean temperature and salinity observations (e.g., from Argos, stations, and expendable probes), providing one of the most comprehensive ocean in situ datasets.

In this study, a window of 20 days before Megi reached typhoon strength on 14 October 2010 is used to search possible temperature profiles that represent pre-Megi ocean conditions. By this strategy, 13 and 5 profiles are obtained in the vicinity of Megi over the Philippine Sea and the South China Sea, respectively (Fig. 1). Not surprisingly, a thick, warm water layer of 119 m, which is defined by the depth of 26°C isotherm (D26), is found in the Philippine Sea, compared to the shallow, warm water layer of 57 m in the South China Sea (Fig. 4). Because of the similarity of the profiles, we arbitrarily choose one profile from each basin as an initial condition for the subsequent numerical experiments. The profiles at 19.0°N, 125.3°E on 14 October and at 18.7°N, 119.5°E on 2 October are selected to represent the ocean conditions of the Philippine Sea and the South China Sea, respectively (solid triangles in Fig. 1 and heavy profiles in Fig. 4).

3. Model and experiment design

a. *3DPWP model*

To examine and quantify the effect of typhoon size on Megi-induced SST cooling, we employ the three-dimensional Price–Weller–Pinkel (3DPWP) ocean-mixing model to conduct a set of numerical experiments. Developed by Price et al. (1994), the 3DPWP has been a widely used physical ocean model to study ocean response to a moving typhoon (e.g., Sanford et al. 2007; Lin et al. 2013; Walker et al. 2014; Guan et al. 2014; Balaguru et al. 2015; Wu et al. 2016; Hsu et al. 2017; Huang et al. 2017). The 3DPWP is a hydrostatic model with primitive equations of temperature, salinity, and momentum budgets. The most important subgrid process in the model is the vertical mixing, which is parameterized by three factors: density-driven static stability, wind-driven entrainment, and vertical shear flow instability. More details can be found in Price et al. (1994) and Lin et al. (2013).

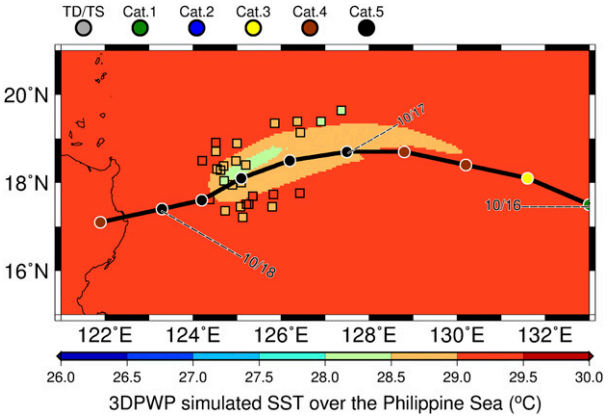

FIG. 5. The 3DPWP simulated SST at 1500 UTC 17 Oct over the Philippine Sea with observed condition (i.e., control experiment). The color-coded squares are the 29 AXBT observations from ITOP. Note that there is no terrain or bathymetry in the 3DPWP. The coastal lines shown here only depict the geographic location.

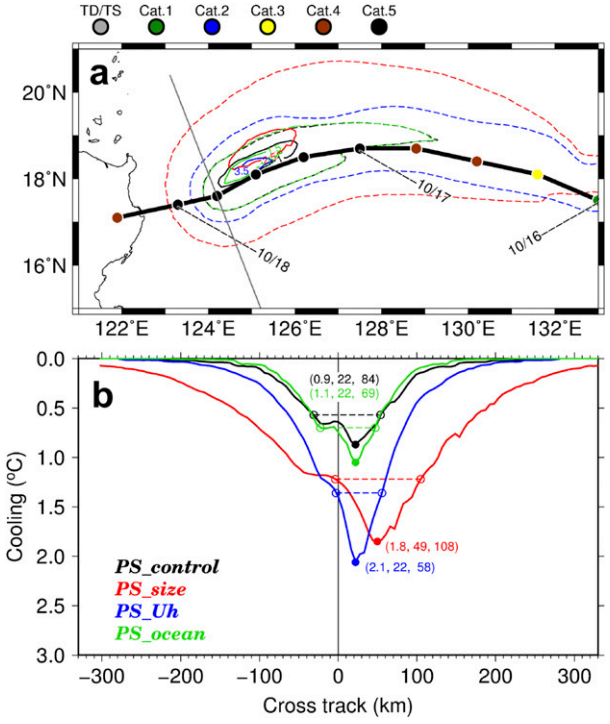

FIG. 6. (a) Simulated SST cooling at 1800 UTC 17 Oct from different experiments over the Philippine Sea. Dashed contours represent 0.5°C cooling, while solid contours represent the core of the cooling. Cross-sectional lines are shown. (b) Cross-track SST cooling at 1800 UTC 17 Oct; the location is depicted by the solid gray line in (a). Solid (open) circles depict the maximum (66%) cooling, while the dashed lines depict the width of the cooling. The numbers in the parentheses are the maximum cooling (°C), right bias (km), and width (km). Note that the coastal lines shown in (a) only depict the geographic location.

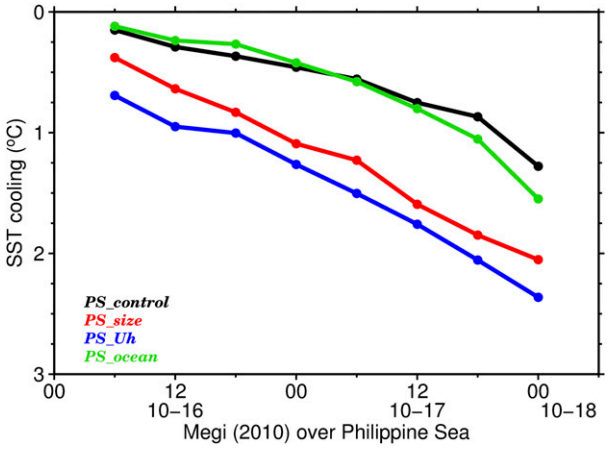

FIG. 7. Along-track SST cooling of the Philippine Sea experiments.

The horizontal resolution of the 3DPWP is 5 km. No terrain and bathymetry are considered. There are 45 layers in the vertical, with 5-, 10-, and 50-m intervals for 0–100, 100–200, and 200–1000 m, respectively. The time interval for the integration is 15 min. Spatial domain for the Philippine Sea (South China Sea) segment of Megi's passage is 15°–21°N and 121°–133°E (15°–21°N and 115°–121°E) (Fig. 1). The initial temperature field is laterally homogeneous, whereas the salinity is kept constant throughout. It should be noted that all air–sea heat exchanges are turned off, and background current is at rest in the present simulations (Lin et al. 2013, 2014; Huang et al. 2015). Therefore, entrainment mixing and upwelling are the only two physical mechanisms for the SST cooling.

b. *Numerical experiments*

As mentioned earlier, Megi's characteristics (e.g., size and translation speed) and the preexisting ocean thermal conditions are quite different over the Philippine Sea and the South China Sea. The main features of Megi between these two basins are summarized in Table 1, based on two specific periods: 1) intensification stage during 0000 UTC 16 October–1200 UTC 17 October, covered by SFMR observations, and 2) maintenance stage during 0000 UTC 20 October–1200 UTC 21 October (cf. Fig. 2). Statistically, the mean radii of Megi are about 227% greater over the South China Sea than those over the Philippine Sea (Table 1, bottom). To provide cross comparisons and determine the relative contributions, the influences of translation speed and ocean components are also examined. Megi's passage is separated into two portions according to the basins (viz., the Philippine Sea and the South China Sea) for carrying out respective numerical experiments.

The first part of the experiments is in the Philippine Sea domain, where Megi underwent the intensification stage with a very small size (Fig. 2). The simulation period for this portion is from 0000 UTC 16 October to 0600 UTC 18 October. The second part is in the South China Sea region, where Megi strengthened to category 4 with a large size (Fig. 2). The simulation period for the South China Sea portion is from 0000 UTC 19 October to 0000 UTC 22 October. For each basin (or track segment), one control experiment (based on observed conditions) and three experiments regarding the size, translation speed, and ocean condition are conducted by using the 3DPWP model (Table 2). Each experiment is conducted by replacing the corresponding values with the values in the other basin according to Table 1. Note that the periods in Table 1 are different from the simulation periods. For example, in the translation speed experiment of the South China Sea (SCS_Uh), the observed speed is replaced with 7.1 m s^{-1}, at which Megi transited over the Philippine Sea. It should be noted that

TABLE 3. Averaged changes and the corresponding percentage (in parentheses) in the maximum SST cooling, right bias, and width of the SST cooling with respect to the control experiment over the Philippine Sea.

Expt	Max SST cooling (°C)	Right bias (km)	Width (km)
PS_size	0.62 (105%)	24.1 (121%)	44.7 (76%)
PS_Uh	0.86 (146%)	−1.4 (−7%)	−15.1 (−26%)
PS_ocean	0.04 (7%)	−1.4 (−7%)	−15.1 (−26%)

Megi's intensity is a function of time in all experiments, which is based on the observations as shown in Fig. 2.

4. Results

a. Philippine Sea experiments

First, the SST cooling induced by Megi in the Philippine Sea is examined at the time when Megi was a fast-moving and compact typhoon. Superimposed with 29 airborne expendable bathythermograph (AXBT) observations on 17 October from ITOP, Fig. 5 shows SST at 1500 UTC 17 October simulated by the 3DPWP model under the observed conditions (i.e., PS_control). It is found that the magnitude and spatial variation of the simulated SST cooling are in good agreement with the AXBT observations. The root-mean-square difference is 0.41°C.

To compare the effects of the typhoon size with the other well-known factors (i.e., translation speed and preexisting ocean conditions), SST cooling is extracted from each experiment (Fig. 6). The control experiment is used as a baseline to quantify the influence of each factor. Here, we consider the during-typhoon SST cooling, as it has an instant impact on typhoon intensification (Cione and Uhlhorn 2003; Zhang et al. 2017). In this context, the SST cooling for each 6-hourly track point is defined as the difference in SST at the time of Megi's position and initial SST (i.e., pre-Megi condition). For example, the SST cooling for Megi's position at 1800 UTC 17 October (Fig. 6) is the SST difference between 1800 UTC 17 October and 0000 UTC 16 October. However, it should be noted that in the translation speed experiments, the model time changes in accordance with the modified translation speed. For the sake of simplicity, the subsequent analyses and comparisons throughout this paper are based on the best track positions and times from IBTrACS. In other words, the same best track times are imposed for each simulation, despite the changed model times due to substituted translation speeds.

Figure 6a compares the SST cooling at Megi's position at 1800 UTC 17 October among the experiments, and varying degrees of change are found in terms of the magnitude and the spatial extent of the cooling pattern. All simulated SST cooling more or less shows a right bias relative to Megi's center, which is consistent with existing observational results (e.g., D'Asaro et al. 2007). The impacts may be more evident in the cooling cross sections perpendicular to Megi's movement (Fig. 6b). In the PS_size experiment, the size of Megi, characterized by RMW, R64, R50, and R34, is artificially expanded by about 227%, roughly equivalent to its size over the South China Sea. The 3DPWP simulation shows that both the magnitude and the extent of the SST cooling increase considerably as Megi enlarges (red vs black curves in Fig. 6; hereafter, the changes are with respect to the control experiment, if not specified). From the cross section in Fig. 6b, it is found that the maximum SST cooling increases by 0.9°C, whereas the width of the SST cooling, which is based on the criterion of 66% of the maximum SST cooling defined by D'Asaro et al. (2014), widens by 24 km. In addition, the right bias slightly shifts by 27 km. In the PS_Uh experiment, in which the translation speed is decreased to 2.6 m s^{-1}, the maximum SST cooling increases significantly to 2.1°C,

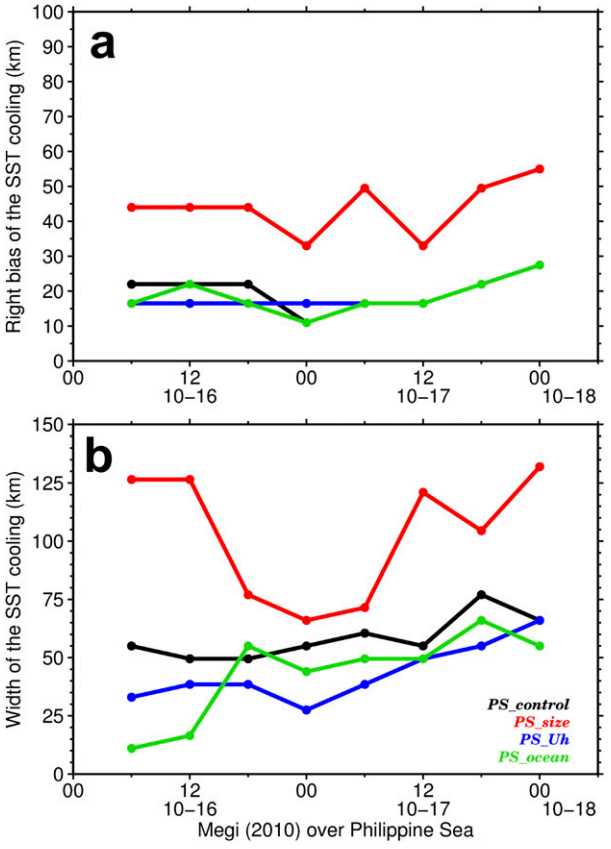

FIG. 8. As in Fig. 7, but for (a) right bias and (b) width of the SST cooling.

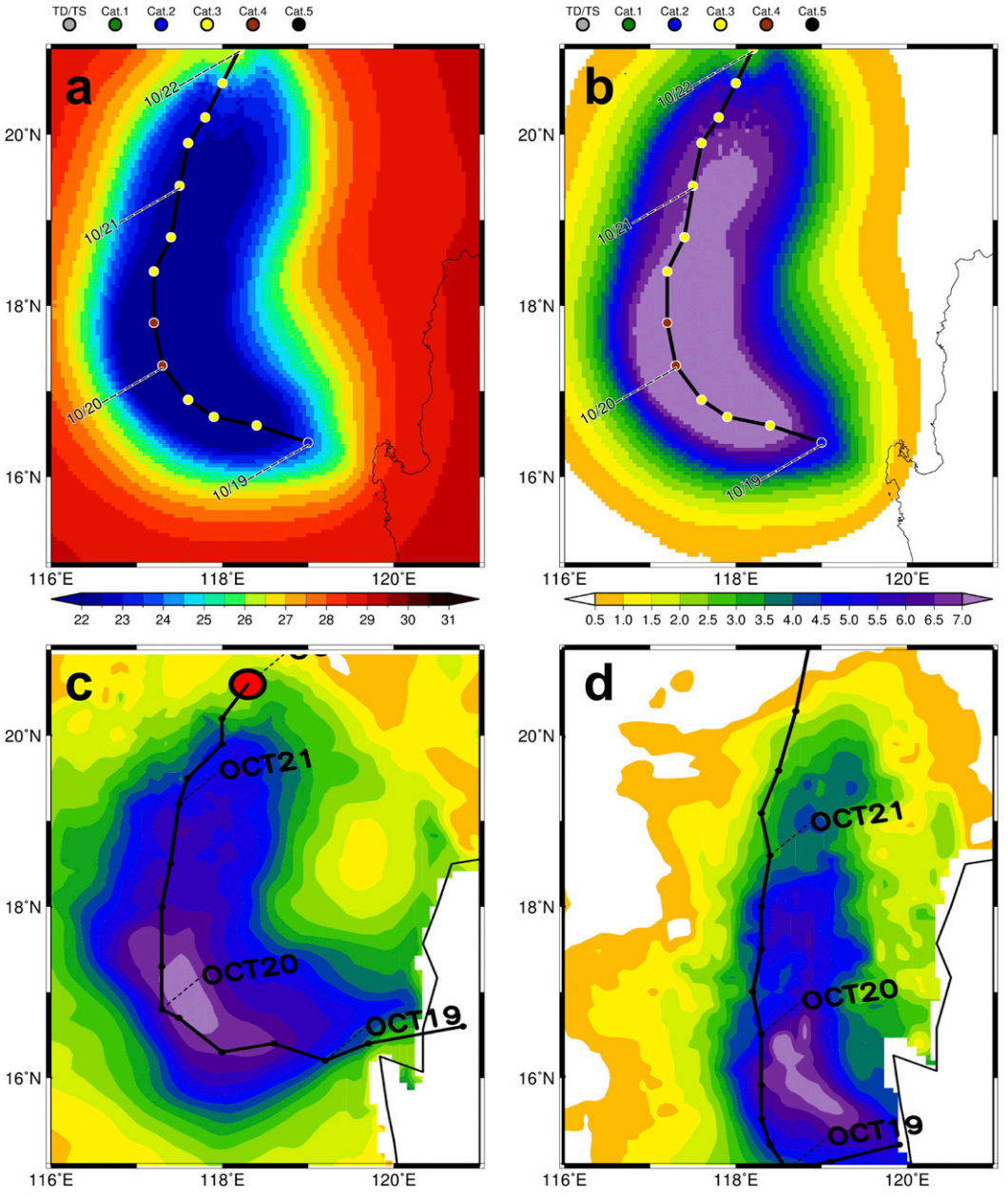

FIG. 9. (a),(b) The simulated SST and SST cooling of the control experiment of the South China Sea (i.e., SCS_control) at 0000 UTC 22 Oct 2010, respectively. (c),(d) The corresponding SST decreases simulated by Eastern Asian Seas Nowcast/Forecast system (EASNFS) and WRF-3DPWP coupled model, respectively [after Wu et al. (2016)]. Same color scale is for (b)–(d). Note that the coastal lines shown in (a),(b) only depict the geographic location.

and the width of SST slightly decreases by 26 km (blue in Fig. 6b). However, the right bias remains unchanged. Finally, in the PS_ocean experiment, in adjusting the upper-ocean thermal structure to the South China Sea conditions (colder subsurface), only the magnitude of the cooling shows modest enhancement, while the width and right bias are barely affected (green in Fig. 6b).

To further quantify the overall impacts of these three factors, the along-track SST cooling from different experiments is compared (Fig. 7). It is noteworthy that the first (0000 UTC 16 October) and the last (0600 UTC 18 October) points are eliminated due to the spinup and land issues. The along-track SST cooling is obtained as the maximum SST cooling along the cross

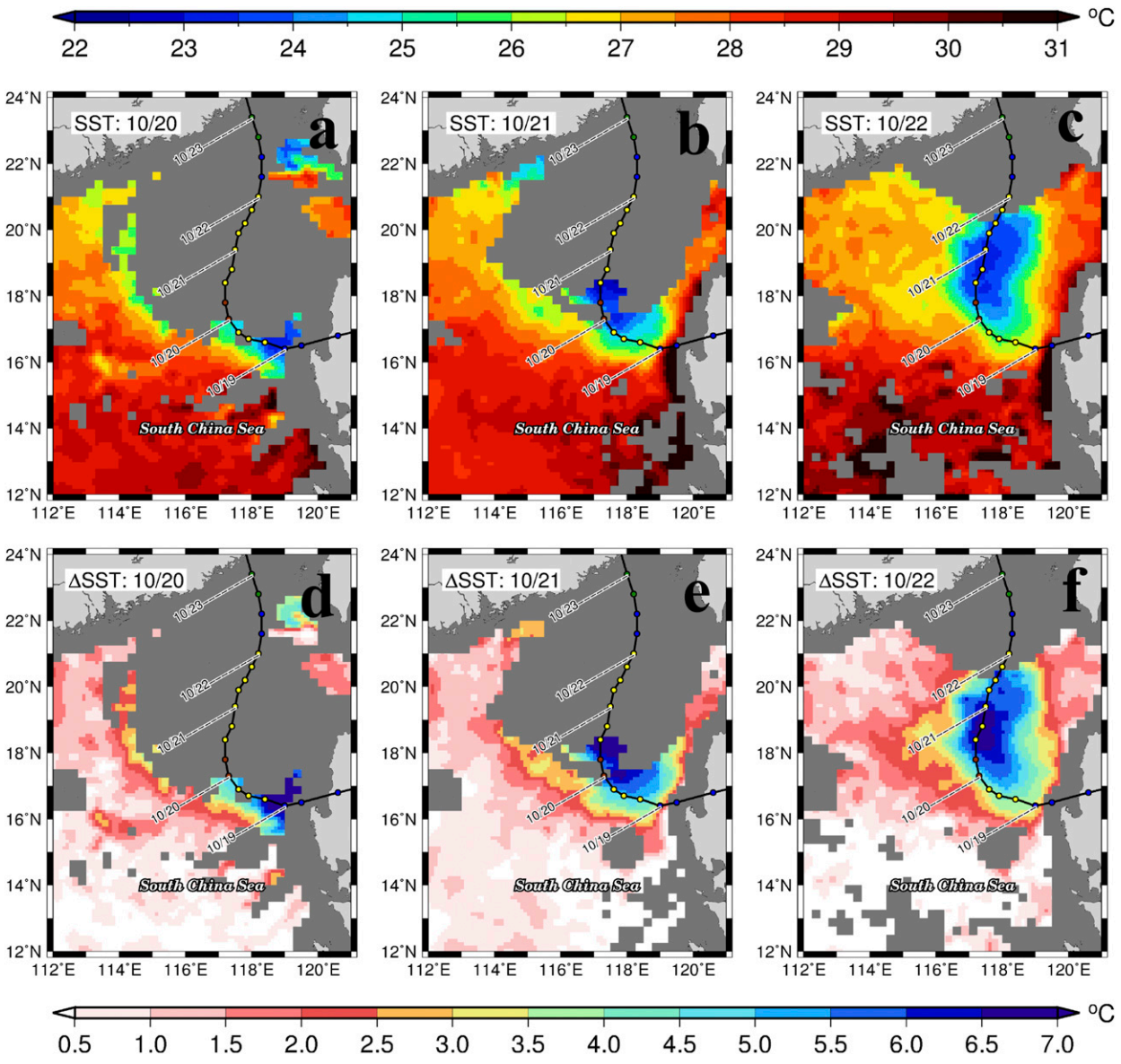

FIG. 10. Series of daily (a)–(c) SST and (d)–(f) SST cooling during 20–22 Oct 2010 over the SCS based on satellite microwave daily composite. The SST cooling is with respect to prestorm SST map on 15 Oct 2010.

sections (cf. Fig. 6b). As seen in Fig. 7, all experiments show an increase in SST cooling as Megi intensifies. However, we found that the impact of translation speed is the most obvious, while the typhoon size has a second large effect. The upper-ocean thermal condition appears to have relatively minor effect. The conditions of the typhoon size, translation speed, and ocean associated with the South China Sea counterpart all act to enhance the SST cooling. On average, they would enhance the cooling by 105%, 146%, and 7%, respectively, over the Philippine Sea if the South China Sea conditions applied (Table 3).

Figure 8 compares the right bias and the width of the SST cooling along Megi's track among all experiments over the Philippine Sea. These two parameters appear more sensitive to the typhoon size. An increase in Megi's size causes the SST cooling to expand in cross-track direction. Slow translation speed and cold ocean thermal conditions tend to reduce the width of the SST cooling. Recall that the width of the cooling is a relative quantity with respect to the maximum cooling (D'Asaro et al. 2014). Based on the 3DPWP simulations, on average, a large typhoon size increases the right bias and the width of the SST cooling by 121% and 76%, respectively,

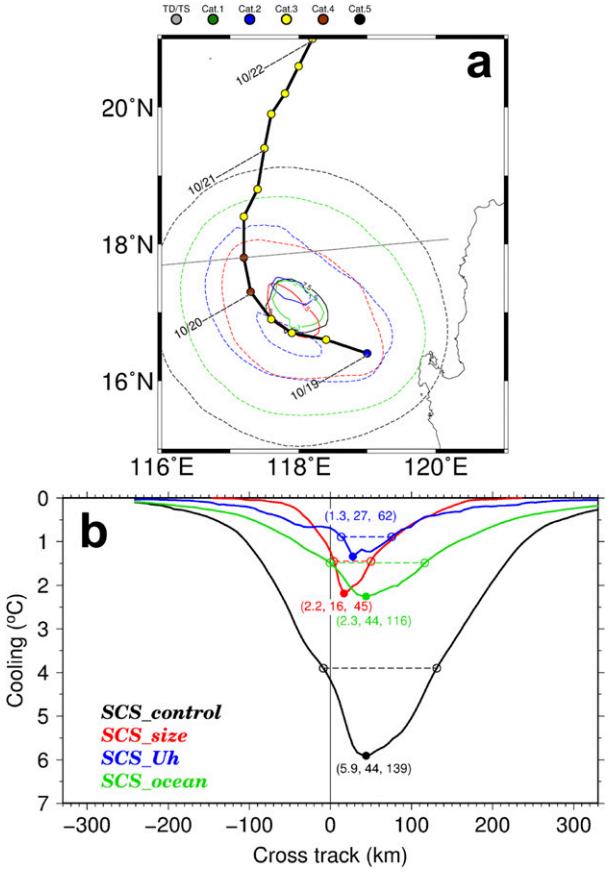

FIG. 11. As in Fig. 6, but for simulated SST cooling at 0600 UTC 20 Oct for the South China Sea experiments.

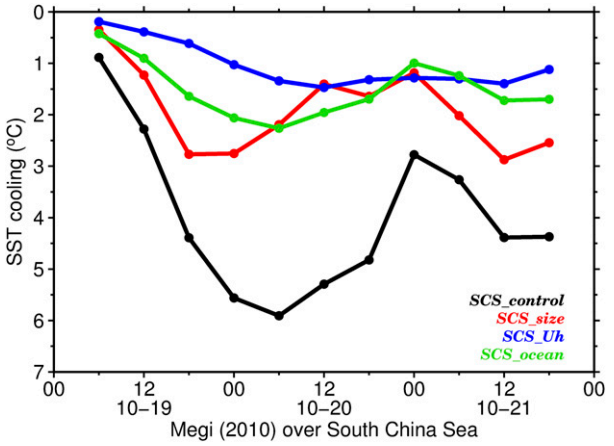

FIG. 12. Along-track SST cooling of the South China Sea experiments.

while slow translation speed and cold ocean thermal conditions both account for 7% and 26% reductions (Table 3).

b. South China Sea experiments

As opposed to the period over the Philippine Sea, Megi turned into a stalling and huge typhoon over the South China Sea (Fig. 2 and Table 1). In the control experiment (i.e., SCS_control; Figs. 9a,b), SST after Megi's passage simulated by the 3DPWP is in good agreement with satellite daily microwave observations (Figs. 10a–c). The modeled SST cooling is around 7°–8°C along the curving track, which is also consistent with the observations (Figs. 10d–f) and existing literature (D'Asaro et al. 2014; Guan et al. 2014). Furthermore, our simulated SST cooling is fairly comparable to the model results of Wu et al. (2016), who used an advanced atmosphere–ocean coupled model with a more sophisticated data assimilated wind field (Figs. 9c,d).

Figure 11 shows the SST cooling of all South China Sea experiments at 0600 UTC 20 October. Similar to the findings in the Philippine Sea, the simulated SST cooling shows rightward bias to some extent. The maximum SST cooling differs significantly among the experiments and occurs in the right rear quadrant behind Megi's passage (Fig. 11a). The pronounced differences can also be seen in the cross section (Fig. 11b). In the typhoon size experiment (i.e., SCS_size), in which the size of Megi is shrunk by about 56%, the magnitude, right bias, and width of SST cooling under the typhoon decrease significantly by 3.7°C, 28 km, and 94 km, respectively, compared to the control experiment (red vs. black curves in Fig. 11b). In the SCS_Uh experiment, in which the translation speed is increased to the value over the Philippine Sea (i.e., 7.1 m s^{-1}), the SST cooling changes even dramatically in terms of the magnitude (blue curve in Fig. 11b). The magnitude of SST cooling under the typhoon decreases sharply from 5.9° to 1.3°C, equivalent to a 78% reduction. The right bias and the width of the cooling decrease by 17 and 77 km, respectively. In the SCS_ocean experiment, substituting with the warmer ocean subsurface condition, there is a 3.6°C reduction in the SST cooling, which is comparable to the typhoon size effect. However, the right bias has no change, and the width decreases moderately by 23 km (green curve in Fig. 11b).

It is clear from the along-track SST cooling shown in Fig. 12 that all three factors act to mitigate the typhoon-induced SST cooling over the South China Sea if

TABLE 4. As in Table 3, but for the South China Sea experiments.

Expt	Max SST cooling (°C)	Right bias (km)	Width (km)
SCS_size	−2.09 (−52%)	−30.0 (−60%)	−52.0 (−61%)
SCS_Uh	−2.95 (−74%)	−5.0 (−10%)	−17.5 (−20%)
SCS_ocean	−2.48 (−62%)	−3.0 (−6%)	5.0 (6%)

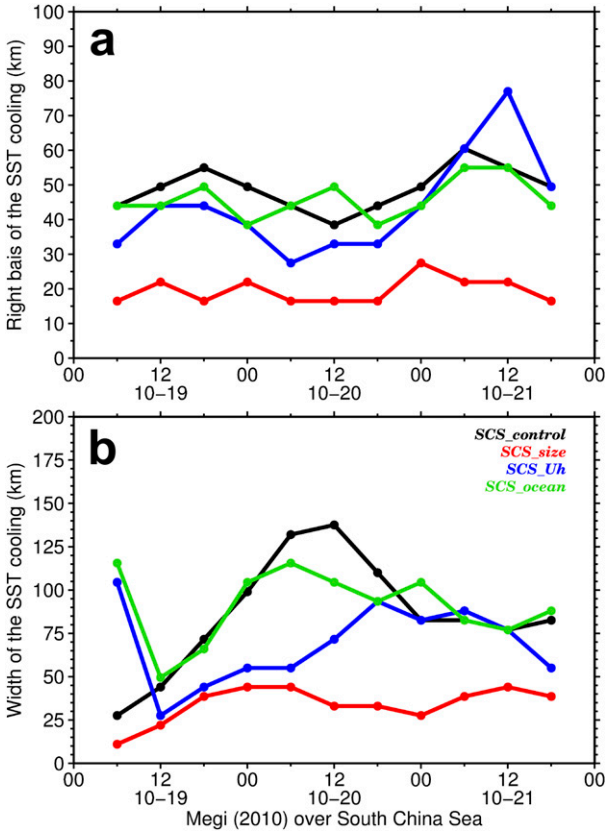

FIG. 13. As in Fig. 12, but for (a) right bias and (b) width of the SST cooling.

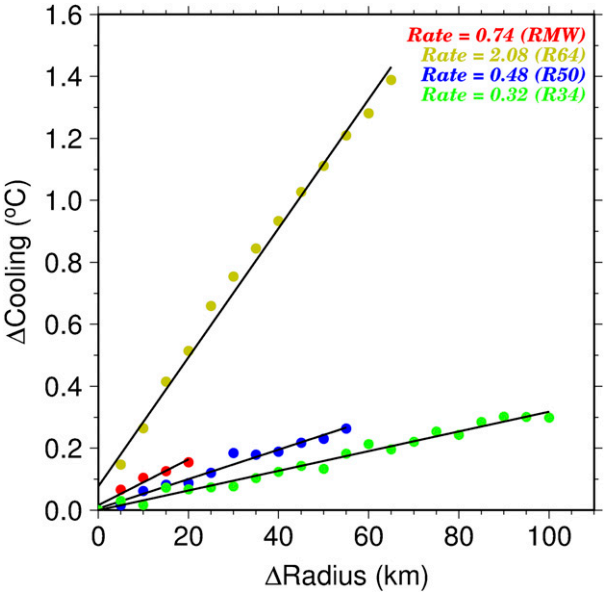

FIG. 14. Rate of change of SST cooling with respect to the change in wind radii of 64 (red), 50 (blue), and 34 (green) kt. The black lines indicate the linear fitting for each group, whereas the corresponding linear rates [i.e., slopes; °C (100 km)$^{-1}$] are also shown.

replaced with Philippine Sea conditions. According to the simulation results, translation speed ranks the most influential factor for the Megi-induced cooling magnitude over the South China Sea: it would lead to a 74% overall reduction (Table 4). Not surprisingly, the ocean thermal condition also plays a determinant role; on average, it would cause a 62% decrease in SST cooling. However, it is noteworthy that the effect of typhoon size is equally important in this case: it would lead to a 52% reduction in SST cooling, from 4° to 1.9°C. In fact, the simultaneous occurrence of large typhoon size, slow translation speed, and colder ocean subsurface conditions allows Megi to generate an immense SST cooling over the South China Sea.

Figure 13 compares the right bias and the width of the SST cooling. Consistent with the results in the Philippine Sea experiments (Fig. 8a), the right bias is more sensitive to the typhoon size while the other two factors show relatively moderate effect (Fig. 13a). In addition, it is evident that smaller typhoon size leads to a narrow cooling in this case (Fig. 13b). However, fast translation speed and colder ocean subsurface conditions tend to reduce the overall width of the SST cooling, which are similar to the outcome from the Philippine Sea experiments (Fig. 8b). The average changes in the right bias and the width of the SST cooling among the South China Sea experiments are summarized in Table 4.

c. *Dependence on typhoon size*

Both sets of experiments have shown that typhoon size has a significant impact on the SST cooling. To quantitatively assess the dependence of the SST cooling on the typhoon size, we conduct experiments that allow a single wind radius (i.e., RMW, R64, R50, and R34) varying over a reasonable range. For instance, the range for R64 is from 55 to 120 km, increasing 5 km each time while keeping the other radii unchanged.

Based on the simulations over the South China Sea, Fig. 14 shows the rate of change in the maximum SST cooling under the typhoon with respect to the change in the size specified by the wind radius. As expected, the rates are nearly linear (Price 1981). It is found that the rate of change is highest for R64 [2.08°C (100 km)$^{-1}$], followed by RMW [0.74°C (100 km)$^{-1}$], R50 [0.48°C (100 km)$^{-1}$], and R34 [0.32°C (100 km)$^{-1}$]. This result is understandable because stronger wind would have greater effect on SST cooling. Based on the cooling rates, the overall contribution to the maximum cooling due to the increase in R64, from the Philippine Sea (52.6 km) to the South China Sea (119.7 km), is 1.4°C. Meanwhile, RMW, R50, and R34 account for 0.18°, 0.57°, and 0.63°C, respectively. The total contribution to

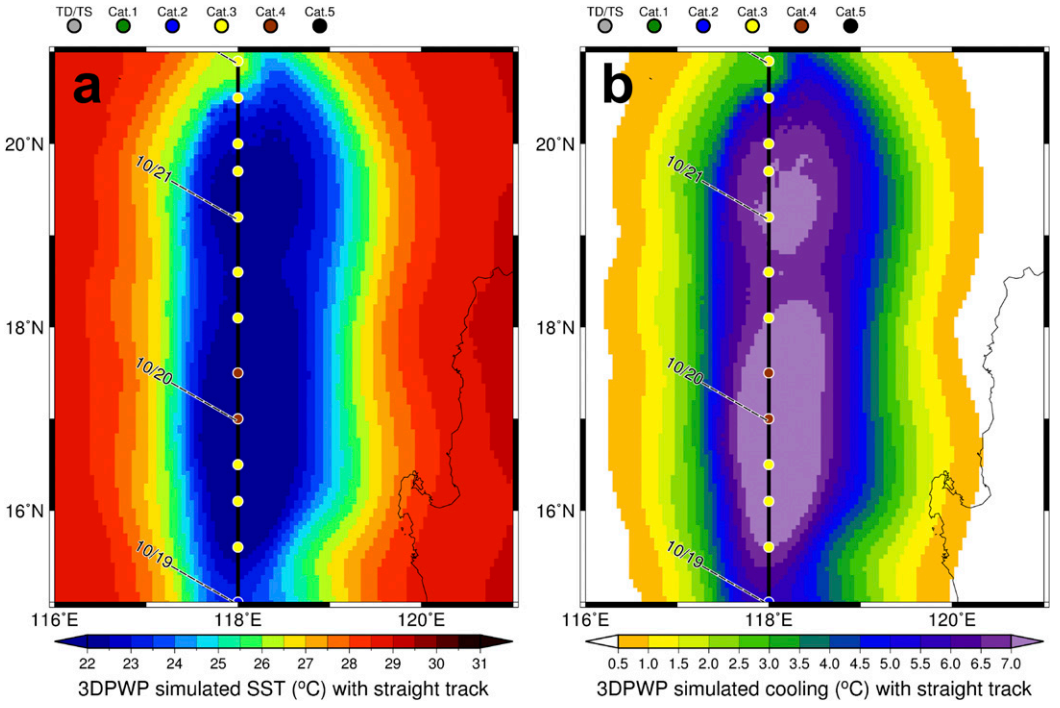

FIG. 15. (a) SST and (b) SST cooling from the straight experiment over the South China Sea. In this experiment, Megi is forced to go straight from the south to the north, while all other conditions are the same as the control experiment (Figs. 9a,b). Note that there is no terrain or bathymetry in the 3DPWP, and the coastal lines only depict the geographic location.

the maximum SST cooling is about 2.78°C, which is generally consistent with the result of the SCS_size experiment (Table 4). However, it should be noted that this assessment is based on an ideally homogenous ocean. In nature, the ocean itself is very dynamic, with features like eddies, so the above rates may be easily changed due to the spatial distribution of such features (Jaimes et al. 2011; Jaimes and Shay 2015).

5. Discussion

a. *Curvature of the track*

Over the South China Sea, Megi made a sharp turn to the north. Large SST cooling appears coincident with the concave side of the curving track (Figs. 9, 10). Apparently, the 3DPWP simulation results show that the SST cooling appears stronger when Megi is curving (1800 UTC 19 October–1800 UTC 20 October; Fig. 12). Given this contrast in the SST cooling, it is interesting to investigate whether the curvature of the typhoon track contributes to SST cooling over the South China Sea. To do so, an additional experiment is conducted by artificially forcing Megi to go straight all the way across the South China Sea, while other conditions are identical to the control experiment (i.e., SCS_control). In the straight experiment, the starting point of 0000 UTC 19 October is relocated to 15°N, 118°E, and then goes straight up to the north along the longitude of 118°E, until the end point of 0000 UTC 22 October.

Figure 15 shows the simulated SST and corresponding SST cooling after the straight-moving Megi. It is somewhat comparable to the result of the control experiment (Figs. 9a,b). It can be seen that the maximum SST cooling occurs around the peak intensity (i.e., 0000 UTC 20 October) with little bias to the right of the track. Interestingly, there is another maximum SST cooling around the point at 2100 UTC 20 October. This is probably due to Megi slowing down again after a short period of speeding up. Notwithstanding, this discussion will be focused on the curvature period, that is, 1800 UTC 19 October–1800 UTC 20 October. The straight-track experiment reveals that the curvature of Megi's track contributes 1.2°C to the maximum SST cooling during the typhoon, which is equivalent to a 30% difference, compared to the control experiment (Fig. 16a). Meanwhile, the curvature also has a significant influence on the right bias and the width of the SST cooling; both are enhanced by 20% and 47%, respectively (Figs. 16b,c).

b. *Size and residence time of the typhoon*

Our simulation results suggest that the translation speed acts as the most important factor responsible for

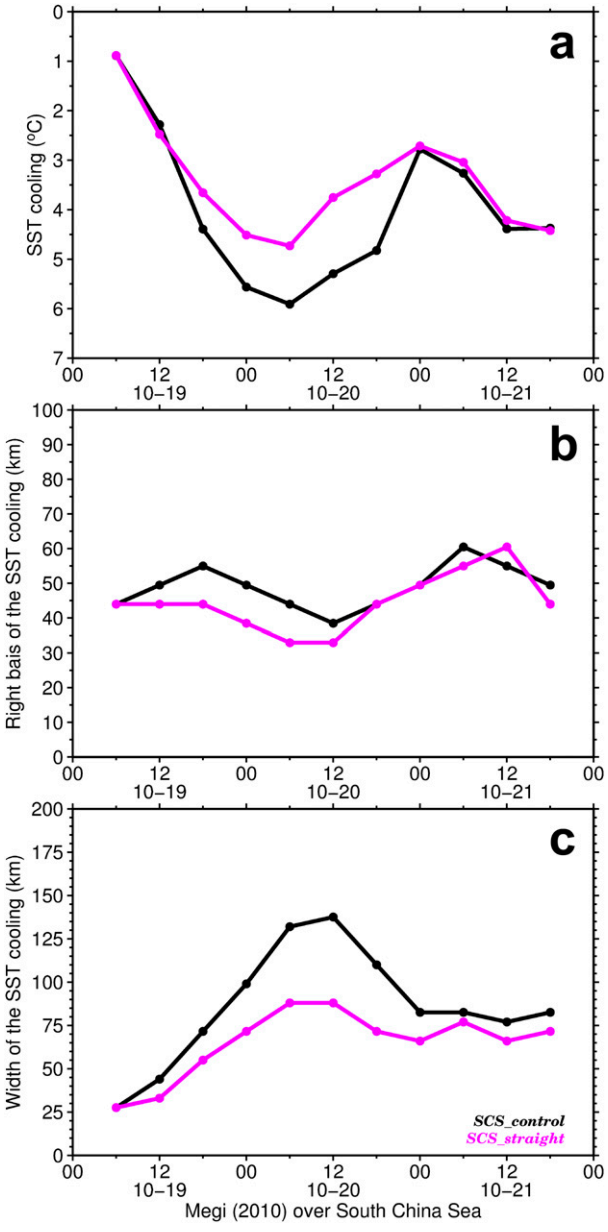

FIG. 16. Comparisons of (a) SST cooling, (b) right bias, and (c) width of the SST cooling between control and straight experiments over the South China Sea.

the distinctive SST cooling induced by Megi over the Philippine Sea and the South China Sea. In fact, the typhoon translation speed is one of the key factors affecting the underlying ocean response (Price 1981; Lin et al. 2009; Mei et al. 2012). This is because the residence time of the typhoon is directly linked to its translation speed. From the ocean perspective, a slow- (fast) moving typhoon has longer (shorter) time to exert forcing on the ocean. As a matter of fact, the residence time is also related to the size and the path of the typhoon (e.g., curvature). Given the typhoon translation speed, Price et al. (1994) used a length scale of 4 times the RMW to define typhoon size for the purpose of calculating the residence time, while Lin et al. (2008) fixed to 220 km for the western North Pacific typhoons. However, the spatial variation of the residence time of strong winds relative to the typhoon passage may be relevant to the spatial distribution of the SST cooling (Sun et al. 2014).

In this context, we experimentally use the radius of 64 kt (R64), that is, typhoon-force winds, to compute the residence time of Megi over the South China Sea and to investigate the impact of typhoon size on the residence time. Based on the satellite-based CIRA radii reanalysis, it is found that the residence time of Megi's wind varies spatially with the maximum of about 28 h, located on the right side of the curving track (Fig. 17a). Not surprisingly, the SST cooling pattern is generally consistent with the residence time (Figs. 9, 10), indicating the importance of this factor. It is noteworthy that the residence time decreases dramatically to about 12 h if the size of Megi is reduced by 56% to the level over the Philippine Sea (Fig. 17b). Price (1983) proposed a nondimensional translation speed S, defined as the ratio of local inertial period ($1/f$) to the typhoon residence time (R64/Uh), in which f is Coriolis frequency and Uh is Megi's translation speed. In fact, this dynamical parameter indicates the resonance between the wind stress and mixed layer near-inertial current, as well as persistence of wind forcing, compared to the local inertial period (D'Asaro et al. 2014). If $S = 1$, the turning of wind stress due to the movement of the typhoon is exactly at the same pace as the turning of the near-inertial current. As a result, the mixed layer current would strengthen and enhance the entrainment mixing. Generally, the resonance would be less effective when S is different from 1. However, if $S < 1$, it indicates that typhoon wind forcing persists longer than the local inertial period. Therefore, the Ekman balance may be established, setting up divergence and upwelling. In this situation, SST cooling may increase, although with less wind current resonance. On the other hand, if $S > 1$, both resonance and upwelling would weaken; thus, less cooling is generated. From Fig. 17c, it is found that Megi is roughly resonant coupling with the near-inertial current over the South China Sea with $S = \sim 1$–1.5. In contrast, S is doubling to >3 because of the decrease in the residence time (Fig. 17d; the size experiment). The large S suggests less entrainment mixing and upwelling, so SST cooling would be weakened. This result supports previous studies (e.g., Price 1981; D'Asaro et al. 2014) that the typhoon size is an important factor in modulating the ocean response to a moving typhoon. However, the relative contribution of entrainment mixing

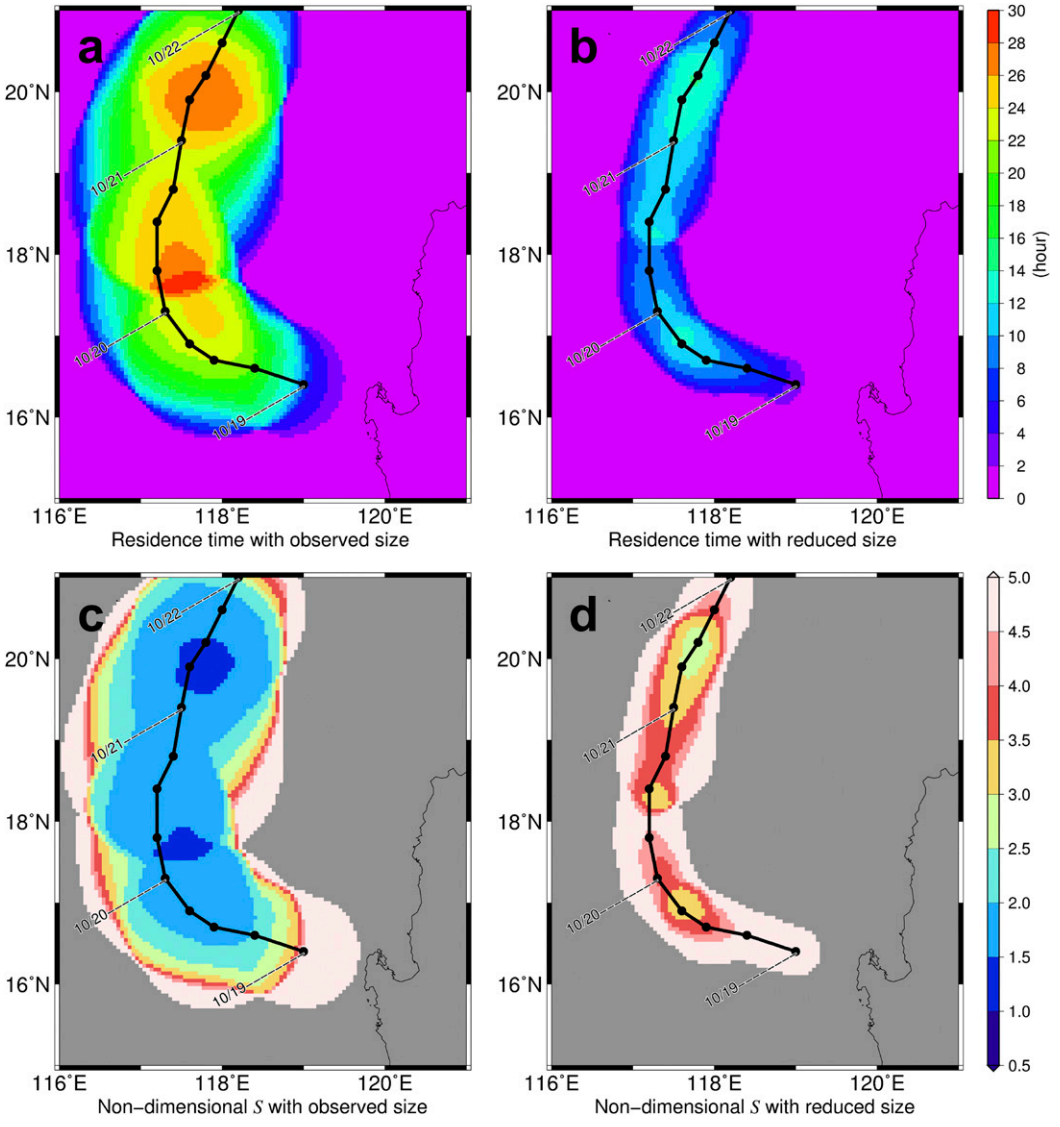

FIG. 17. The residence time of Megi over the South China Sea with (a) observed and (b) reduced (by 56%) cyclone size. (c),(d) The corresponding nondimensional translation speeds S. It can be seen that the residence time and S are strongly linked to the typhoon size.

and upwelling due to the typhoon size variation requires further investigation.

6. Conclusions

Supertyphoon Megi (2010) induced two very contrasting SST coolings over the Philippine Sea and the South China Sea (1.5° vs 7°C). Other than the well-known factors, such as the typhoon translation speed and ocean thermal conditions, this study emphasizes the influence of the typhoon size on SST cooling, especially during Megi's passage. The numerical results suggest that Megi's size has a significant impact on SST cooling, though the translation speed is the main driver for the different ocean responses. In general, large size, slow translation speed, and cold ocean subsurface conditions together allow Megi to generate strong SST cooling over the South China Sea. The opposite is true for its journey over the Philippine Sea. In summary, the magnitude of SST cooling under the typhoon is proportional to the typhoon size but inversely proportional to the translation speed and ocean subsurface thermal condition. These findings are consistent with the previous studies on posttyphoon SST cooling (or cold wake) (e.g., Price 1981; Lin et al. 2008, 2009; D'Asaro et al. 2014). Moreover, the right bias and the

width of the SST cooling also appear sensitive to the typhoon size, both increasing with large typhoon size. Based on the sensitivity tests with an idealized ocean, we found that SST cooling changes linearly with RMW, R64, R50, and R34 during the typhoon, given other factors remain unchanged. The largest rate is for R64 [2.08°C $(100\,\text{km})^{-1}$], followed by RMW [0.74°C $(100\,\text{km})^{-1}$], R50 [0.48°C $(100\,\text{km})^{-1}$], and R34 [0.32°C $(100\,\text{km})^{-1}$].

We have illustrated that the residence time of typhoon-force (64 kt) wind is closely linked to the typhoon size. Given the translation speed, bigger typhoon size leads to longer residence time. The prolonged residence time decreases the nondimensional translation speed, $S = \sim 1$–1.5. In this circumstance, Megi's wind is roughly resonant with the mixed layer current and enhances the upwelling. It may partially explain the extensive SST cooling it left in the South China Sea. In addition, we discovered that the curvature of Megi's track also play a role, contributing up to 30% of the SST cooling over the South China Sea.

Although the findings of the present study are based on numerical experiments and one specific typhoon case, they provide some insight into the importance of typhoon size on during- or posttyphoon SST cooling. As the ocean thermal information has been continuously improved based on satellite techniques (Pun et al. 2014, 2016), typhoon-induced SST cooling can be more accurately estimated by further considering the typhoon size variability. The current results also imply that the typhoon size and track need to be correct in the typhoon prediction models; otherwise, the SST cooling may not be accurate enough to predict subsequent typhoon intensity change. On a longer time scale, how the typhoon size changes in the future climate may play along with other environmental variations, such as ocean subsurface warming (Pun et al. 2013; Lin and Chan 2015). However, the impacts of typhoon size, as well as curvature on ocean response, especially in terms of vertical mixing and upwelling, deserve more in-depth investigations, which will be our topic of future research.

Acknowledgments. We especially thank Dr. James F. Price of WHOI for providing the 3DPWP ocean mixing model and for his insightful comments. Also, we are grateful for the detailed and perspective comments from three anonymous reviewers that helped enhance the quality of this work. Thanks also to the ITOP team and to NOAA/HRD for the excellent SFMR measurements, IBTrACS for the best track data, CIRA for the satellite-based wind radii reanalysis, GTSPP for the in situ ocean temperature profiles, and RSS for the satellite microwave SST data. IFP is supported by Grant MOST 107-2111-M-008-001-MY3. IIL is supported by Grant NSC 103–2111-M-002–002-MY3. CCW is supported by Grant MOST 106-2111-M-002–013-MY3.

REFERENCES

Balaguru, K., G. R. Foltz, L. R. Leung, E. D'Asaro, K. A. Emanuel, H. Liu, and S. E. Zedler, 2015: Dynamic Potential Intensity: An improved representation of the ocean's impact on tropical cyclones. *Geophys. Res. Lett.*, **42**, 6739–6746, https://doi.org/10.1002/2015GL064822.

Bender, M. A., I. Ginis, and Y. Kurihara, 1993: Numerical simulations of tropical cyclone-ocean interaction with a high-resolution coupled model. *J. Geophys. Res.*, **98**, 23 245–23 263, https://doi.org/10.1029/93JD02370.

Black, P. G., and Coauthors, 2007: Air–sea exchange in hurricanes: Synthesis of observations from the Coupled Boundary Layer Air–Sea Transfer Experiment. *Bull. Amer. Meteor. Soc.*, **88**, 357–374, https://doi.org/10.1175/BAMS-88-3-357.

Chan, K. T. F., and J. C. L. Chan, 2013: Angular momentum transports and synoptic flow patterns associated with tropical cyclone size change. *Mon. Wea. Rev.*, **141**, 3985–4007, https://doi.org/10.1175/MWR-D-12-00204.1.

——, and ——, 2014: Impacts of initial vortex size and planetary vorticity on tropical cyclone size. *Quart. J. Roy. Meteor. Soc.*, **140**, 2235–2248, https://doi.org/10.1002/qj.2292.

Chang, S. W., and R. A. Anthes, 1979: The mutual response of the tropical cyclone and the ocean. *J. Phys. Oceanogr.*, **9**, 128–135, https://doi.org/10.1175/1520-0485(1979)009<0128:TMROTT>2.0.CO;2.

Chen, S. S., J. F. Price, W. Zhao, M. Donelan, and E. J. Walsh, 2007: The CBLAST-Hurricane program and the next-generation fully coupled atmosphere–wave–ocean models for hurricane research and prediction. *Bull. Amer. Meteor. Soc.*, **88**, 311–317, https://doi.org/10.1175/BAMS-88-3-311.

Chou, K.-H., C.-C. Wu, P.-H. Lin, and S. Majumdar, 2010: Validation of QuikSCAT wind vectors by dropwindsonde data from Dropwindsonde Observations for Typhoon Surveillance Near the Taiwan Region (DOTSTAR). *J. Geophys. Res.*, **115**, D02109, https://doi.org/10.1029/2009JD012131.

Cione, J. J., and E. Uhlhorn, 2003: Sea surface temperature variability in hurricanes: Implications with respect to intensity change. *Mon. Wea. Rev.*, **131**, 1783–1796, https://doi.org/10.1175//2562.1.

——, P. G. Black, and S. H. Houston, 2000: Surface observations in the hurricane environment. *Mon. Wea. Rev.*, **128**, 1550–1561, https://doi.org/10.1175/1520-0493(2000)128<1550:SOITHE>2.0.CO;2.

D'Asaro, E. A., 2003: The ocean boundary layer below Hurricane Dennis. *J. Phys. Oceanogr.*, **33**, 561–579, https://doi.org/10.1175/1520-0485(2003)033<0561:TOBLBH>2.0.CO;2.

——, T. B. Sanford, P. Niiler, and E. Terrill, 2007: Cold wake of Hurricane Frances. *Geophys. Res. Lett.*, **34**, L15609, https://doi.org/10.1029/2007GL030160.

D'Asaro, E., and Coauthors, 2011: Typhoon-ocean interaction in the western North Pacific: Part 1. *Oceanography*, **24**, 24–31, https://doi.org/10.5670/oceanog.2011.91.

——, and Coauthors, 2014: Impact of typhoons on the ocean in the Pacific. *Bull. Amer. Meteor. Soc.*, **95**, 1405–1418, https://doi.org/10.1175/BAMS-D-12-00104.1.

Elsberry, R. L., T. S. Fraim, and R. N. Trapnell Jr., 1976: A mixed layer model of the oceanic thermal response to hurricanes. *J. Geophys. Res.*, **81**, 1153–1162, https://doi.org/10.1029/JC081i006p01153.

Emanuel, K. A., 1999: Thermodynamic control of hurricane intensity. *Nature*, **401**, 665–669, https://doi.org/10.1038/44326.

Guan, S., W. Zhao, J. Huthnance, J. Tian, and J. Wang, 2014: Observed upper ocean response to Typhoon Megi (2010) in the northern South China Sea. *J. Geophys. Res. Oceans*, **119**, 3134–3157, https://doi.org/10.1002/2013JC009661.

Hsu, J., R. Lien, E. A. D'Asaro, and T. B. Sanford, 2017: Estimates of surface wind stress and drag coefficients in Typhoon Megi. *J. Phys. Oceanogr.*, **47**, 545–565, https://doi.org/10.1175/JPO-D-16-0069.1.

Huang, H.-C., J. Boucharel, I.-I. Lin, F.-F. Jin, C.-C. Lien, and I.-F. Pun, 2017: Air-sea fluxes for Hurricane Patricia (2015): Comparison with supertyphoon Haiyan (2013) and under different ENSO conditions. *J. Geophys. Res. Oceans*, **122**, 6076–6089, https://doi.org/10.1002/2017JC012741.

Huang, P., I. I. Lin, C. Chou, and R. H. Huang, 2015: Change in ocean subsurface environment to suppress tropical cyclone intensification under global warming. *Nat. Commun.*, **6**, 7188, https://doi.org/10.1038/ncomms8188.

Jacob, S. D., L. K. Shay, A. J. Mariano, and P. G. Black, 2000: The 3D oceanic mixed layer response to Hurricane Gilbert. *J. Phys. Oceanogr.*, **30**, 1407–1429, https://doi.org/10.1175/1520-0485(2000)030<1407:TOMLRT>2.0.CO;2.

Jaimes, B., and L. K. Shay, 2009: Mixed layer cooling in mesoscale oceanic eddies during Hurricanes Katrina and Rita. *Mon. Wea. Rev.*, **137**, 4188–4207, https://doi.org/10.1175/2009MWR2849.1.

——, and ——, 2010: Near-inertial wave wake of Hurricanes Katrina and Rita in mesoscale oceanic eddies. *J. Phys. Oceanogr.*, **40**, 1320–1337, https://doi.org/10.1175/2010JPO4309.1.

——, and ——, 2015: Enhanced wind-driven downwelling flow in warm oceanic eddy features during the intensification of Tropical Cyclone Isaac (2012): Observations and theory. *J. Phys. Oceanogr.*, **45**, 1667–1689, https://doi.org/10.1175/JPO-D-14-0176.1.

——, ——, and G. R. Halliwell, 2011: The response of quasi-geostrophic oceanic vortices to tropical cyclone forcing. *J. Phys. Oceanogr.*, **41**, 1965–1985, https://doi.org/10.1175/JPO-D-11-06.1.

——, ——, and E. W. Uhlhorn, 2015: Enthalpy and momentum fluxes during Hurricane Earl relative to underlying ocean features. *Mon. Wea. Rev.*, **143**, 111–131, https://doi.org/10.1175/MWR-D-13-00277.1.

Klotz, B. W., and E. W. Uhlhorn, 2014: Improved stepped frequency microwave radiometer tropical cyclone surface winds in heavy precipitation. *J. Atmos. Oceanic Technol.*, **31**, 2392–2408, https://doi.org/10.1175/JTECH-D-14-00028.1.

Knapp, K. R., M. C. Kruk, D. H. Levinson, H. J. Diamond, and C. J. Neumann, 2010: The International Best Track Archive for Climate Stewardship (IBTrACS): Unifying tropical cyclone data. *Bull. Amer. Meteor. Soc.*, **91**, 363–376, https://doi.org/10.1175/2009BAMS2755.1.

Ko, D.-S., S.-Y. Chao, C.-C. Wu, and I.-I. Lin, 2014: Impacts of Typhoon Megi (2010) on the South China Sea. *J. Geophys. Res. Oceans*, **119**, 4474–4489, https://doi.org/10.1002/2013JC009785.

Lee, C.-Y., and S. S. Chen, 2014: Stable boundary layer and its impact on tropical cyclone structure in a coupled atmosphere–ocean model. *Mon. Wea. Rev.*, **142**, 1927–1944, https://doi.org/10.1175/MWR-D-13-00122.1.

Leipper, D. F., 1967: Observed ocean conditions and Hurricane Hilda, 1964. *J. Atmos. Sci.*, **24**, 182–186, https://doi.org/10.1175/1520-0469(1967)024<0182:OOCAHH>2.0.CO;2.

Lin, I. I., and J. C. L. Chan, 2015: Recent decrease in typhoon destructive potential and global warming implications. *Nat. Commun.*, **6**, 7182, https://doi.org/10.1038/ncomms8182.

——, W. T. Liu, C. C. Wu, J. C. H. Chiang, and C. H. Sui, 2003: Satellite observations of modulation of surface winds by typhoon-induced upper ocean cooling. *Geophys. Res. Lett.*, **30**, 1131, https://doi.org/10.1029/2002GL015674.

——, C.-C. Wu, K. A. Emanuel, I.-H. Lee, C.-R. Wu, and I. F. Pun, 2005: The interaction of Supertyphoon Maemi (2003) with a warm ocean eddy. *Mon. Wea. Rev.*, **133**, 2635–2649, https://doi.org/10.1175/MWR3005.1.

——, C. C. Wu, I. F. Pun, and D. S. Ko, 2008: Upper-ocean thermal structure and the western North Pacific category 5 typhoons. Part I: Ocean features and the category 5 typhoons' intensification. *Mon. Wea. Rev.*, **136**, 3288–3306, https://doi.org/10.1175/2008MWR2277.1.

——, I. F. Pun, and C. C. Wu, 2009: Upper-ocean thermal structure and the western North Pacific category 5 typhoons. Part II: Dependence on translation speed. *Mon. Wea. Rev.*, **137**, 3744–3757, https://doi.org/10.1175/2009MWR2713.1.

——, and Coauthors, 2013: An ocean coupling potential intensity index for tropical cyclones. *Geophys. Res. Lett.*, **40**, 1878–1882, https://doi.org/10.1002/grl.50091.

——, I. F. Pun, and C.-C. Lien, 2014: "Category-6" Supertyphoon Haiyan in global warming hiatus: Contribution from subsurface ocean warming. *Geophys. Res. Lett.*, **41**, 8547–8553, https://doi.org/10.1002/2014GL061281.

Liu, W. T., and W. Tang, 1996: Equivalent neutral wind. JPL Publ. 96-17, 16 pp., https://ntrs.nasa.gov/archive/nasa/casi.ntrs.nasa.gov/19970010322.pdf.

Mei, W., C. Pasquero, and F. Primeau, 2012: The effect of translation speed upon the intensity of tropical cyclones over the tropical ocean. *Geophys. Res. Lett.*, **39**, L07801, https://doi.org/10.1029/2011GL050765.

Mrvaljevic, R. K., and Coauthors, 2013: Observations of the cold wake of Typhoon Fanapi (2010). *Geophys. Res. Lett.*, **40**, 316–321, https://doi.org/10.1029/2012GL054282.

Mueller, K. J., M. DeMaria, J. Knaff, J. P. Kossin, and T. H. Vonder Haar, 2006: Objective estimation of tropical cyclone wind structure from infrared satellite data. *Wea. Forecasting*, **21**, 990–1005, https://doi.org/10.1175/WAF955.1.

Price, J. F., 1981: Upper ocean response to a hurricane. *J. Phys. Oceanogr.*, **11**, 153–175, https://doi.org/10.1175/1520-0485(1981)011<0153:UORTAH>2.0.CO;2.

——, 1983: Internal wave wake of a moving storm. Part I: Scales, energy budget and observations. *J. Phys. Oceanogr.*, **13**, 949–965, https://doi.org/10.1175/1520-0485(1983)013<0949:IWWOAM>2.0.CO;2.

——, T. B. Sanford, and G. Z. Forristall, 1994: Forced stage response to a moving hurricane. *J. Phys. Oceanogr.*, **24**, 233–260, https://doi.org/10.1175/1520-0485(1994)024<0233:FSRTAM>2.0.CO;2.

——, J. Morzel, and P. P. Niiler, 2008: Warming of SST in the cool wake of a moving hurricane. *J. Geophys. Res.*, **113**, C07010, https://doi.org/10.1029/2007JC004393.

Pun, I. F., I. I. Lin, C. R. Wu, D. H. Ko, and W. T. Liu, 2007: Validation and application of altimetry-derived upper ocean thermal structure in the western North Pacific Ocean for typhoon-intensity forecast. *IEEE Trans. Geosci. Remote Sens.*, **45**, 1616–1630, https://doi.org/10.1109/TGRS.2007.895950.

——, Y. T. Chang, I. I. Lin, T. Y. Tang, and R. C. Lien, 2011: Typhoon–ocean interaction in the western North Pacific: Part 2. *Oceanography*, **24**, 32–41, https://doi.org/10.5670/oceanog.2011.92.

——, I. I. Lin, and M. H. Lo, 2013: Recent increase in high tropical cyclone heat potential area in the western North Pacific Ocean. *Geophys. Res. Lett.*, **40**, 4680–4684, https://doi.org/10.1002/grl.50548.

——, ——, and D. S. Ko, 2014: New generation of satellite-derived ocean thermal structure for the western North Pacific typhoon intensity forecasting. *Prog. Oceanogr.*, **121**, 109–124, https://doi.org/10.1016/j.pocean.2013.10.004.

——, J. F. Price, and S. R. Jayne, 2016: Satellite-derived ocean thermal structure for the North Atlantic hurricane season. *Mon. Wea. Rev.*, **144**, 877–896, https://doi.org/10.1175/MWR-D-15-0275.1.

Sanford, T. B., P. G. Black, J. Haustein, J. W. Feeney, G. Z. Forristall, and J. F. Price, 1987: Ocean response to a hurricane. Part I: Observations. *J. Phys. Oceanogr.*, **17**, 2065–2083, https://doi.org/10.1175/1520-0485(1987)017<2065:ORTAHP>2.0.CO;2.

——, J. Price, J. Girton, and D. Webb, 2007: Highly resolved observations and simulations of the ocean response to a hurricane. *Geophys. Res. Lett.*, **34**, L13604, https://doi.org/10.1029/2007GL029679.

——, ——, and ——, 2011: Upper-ocean response to Hurricane Frances (2004) observed by profiling EM-APEX floats. *J. Phys. Oceanogr.*, **41**, 1041–1056, https://doi.org/10.1175/2010JPO4313.1.

Schade, L., and K. Emanuel, 1999: The ocean's effect on the intensity of tropical cyclones: Results from a simple coupled atmosphere–ocean model. *J. Atmos. Sci.*, **56**, 642–651, https://doi.org/10.1175/1520-0469(1999)056<0642:TOSEOT>2.0.CO;2.

Shay, L. K., P. G. Black, A. J. Mariano, J. D. Hawkins, and R. L. Elsberry, 1992: Upper ocean response to Hurricane Gilbert. *J. Geophys. Res.*, **97**, 20 227–20 248, https://doi.org/10.1029/92JC01586.

——, G. J. Goni, and P. G. Black, 2000: Effects of a warm oceanic feature on Hurricane Opal. *Mon. Wea. Rev.*, **128**, 1366–1383, https://doi.org/10.1175/1520-0493(2000)128<1366:EOAWOF>2.0.CO;2.

Sun, C., and Coauthors, 2010: The data management system for the Global Temperature and Salinity Profile Programme. *Proc. OceanObs'09: Sustained Ocean Observations and Information for Society*, J. Hall, D. E. Harrison, and D. Stammer, Eds., Vol. 2, ESA Publ. WPP-306, https://doi.org/10.5270/OceanObs09.cwp.86.

Sun, L., Y.-X. Li, Y.-J. Yang, Q. Wu, X.-T. Chen, Q.-Y. Li, Y.-B. Li, and T. Xian, 2014: Effects of super typhoons on cyclonic ocean eddies in the western North Pacific: A satellite data-based evaluation between 2000 and 2008. *J. Geophys. Res. Oceans*, **119**, 5585–5598, https://doi.org/10.1002/2013JC009575.

Uhlhorn, E. W., and P. G. Black, 2003: Verification of remotely sensed sea surface winds in hurricanes. *J. Atmos. Oceanic Technol.*, **20**, 99–116, https://doi.org/10.1175/1520-0426(2003)020<0099:VORSSS>2.0.CO;2.

——, and L. K. Shay, 2012: Loop Current mixed layer response to Hurricane Lili (2002). Part I: Observations. *J. Phys. Oceanogr.*, **42**, 400–419, https://doi.org/10.1175/JPO-D-11-096.1.

——, P. G. Black, J. L. Franklin, M. Goodberlet, J. Carswell, and A. S. Goldstein, 2007: Hurricane surface wind measurements from an operational stepped frequency microwave radiometer. *Mon. Wea. Rev.*, **135**, 3070–3085, https://doi.org/10.1175/MWR3454.1.

Vincent, E. M., M. Lengaigne, G. Madec, J. Vialard, G. Samson, N. C. Jourdain, C. E. Menkes, and S. Jullien, 2012: Processes setting the characteristics of sea surface cooling induced by tropical cyclones. *J. Geophys. Res.*, **117**, C02020, https://doi.org/10.1029/2011JC007396.

Wada, A., 2005: Numerical simulations of sea surface cooling by a mixed layer model during the passage of Typhoon Rex. *J. Oceanogr.*, **61**, 41–57, https://doi.org/10.1007/s10872-005-0018-2.

Walker, N. D., R. R. Leben, and S. Balasubramanian, 2005: Hurricane-forced upwelling and chlorophyll *a* enhancement within cold-core cyclones in the Gulf of Mexico. *Geophys. Res. Lett.*, **32**, L18610, https://doi.org/10.1029/2005GL023716.

——, ——, C. T. Pilley, M. Shannon, D. C. Herndon, I.-F. Pun, I.-I. Lin, and C. L. Gentemann, 2014: Slow translation speed causes rapid collapse of northeast Pacific Hurricane Kenneth over cold core eddy. *Geophys. Res. Lett.*, **41**, 7595–7601, https://doi.org/10.1002/2014GL061584.

Wang, Y., and C.-C. Wu, 2004: Current understanding of tropical cyclone structure and intensity changes—A review. *Meteor. Atmos. Phys.*, **87**, 257–278, https://doi.org/10.1007/s00703-003-0055-6.

Wu, C.-C., K.-H. Chou, H.-J. Cheng, and Y. Wang, 2003: Eyewall contraction, breakdown and reformation in a landfalling typhoon. *Geophys. Res. Lett.*, **30**, 1887, https://doi.org/10.1029/2003GL017653.

——, C.-Y. Lee, and I.-I. Lin, 2007: The effect of the ocean eddy on tropical cyclone intensity. *J. Atmos. Sci.*, **64**, 3562–3578, https://doi.org/10.1175/JAS4051.1.

——, W.-T. Tu, I.-F. Pun, I.-I. Lin, and M. S. Peng, 2016: Tropical cyclone-ocean interaction in Typhoon Megi (2010)—A synergy study based on ITOP observations and atmosphere-ocean coupled model simulations. *J. Geophys. Res. Atmos.*, **121**, 153–167, https://doi.org/10.1002/2015JD024198.

Yablonsky, R. M., and I. Ginis, 2013: Impact of a warm ocean eddy's circulation on hurricane-induced sea surface cooling with implications for hurricane intensity. *Mon. Wea. Rev.*, **141**, 997–1021, https://doi.org/10.1175/MWR-D-12-00248.1.

Zhang, J. A., J. J. Cione, E. A. Kalina, E. W. Uhlhorn, T. Hock, and J. A. Smith, 2017: Observations of infrared sea surface temperature and air–sea interaction in Hurricane Edouard (2014) using GPS dropsondes. *J. Atmos. Oceanic Technol.*, **34**, 1333–1349, https://doi.org/10.1175/JTECH-D-16-0211.1.

Zheng, Z.-W., I.-I. Lin, B. Wang, H.-C. Huang, and C.-H. Chen, 2015: A long neglected damper in the El Niño–typhoon relationship: A 'Gaia-like' process. *Sci. Rep.*, **5**, 11 103, https://doi.org/10.1038/srep11103.